

Looking for a Needle in a Haystack? Look Elsewhere!

A statistical comparison of approximate global p-values.

Sara Algeri ^{a,1,2}, David A. van Dyk ^{b,1}, Jan Conrad ^{c,2,3,4,1}, Brandon Anderson ^{d,2,3}

¹Department of Mathematics, Imperial College London, South Kensington Campus, London SW7 2AZ, United Kingdom

²Department of Physics, Stockholm University, AlbaNova, SE-106 91 Stockholm, Sweden

³The Oskar Klein Centre for Cosmoparticle Physics, AlbaNova, SE-106 91 Stockholm, Sweden

⁴Wallenberg Academy Fellow

Received: date / Accepted: date

Abstract The search for new significant peaks over a energy spectrum often involves a statistical multiple hypothesis testing problem. Separate tests of hypothesis are conducted at different locations producing an ensemble of local p-values, the smallest of which is reported as evidence for the new resonance. Unfortunately, controlling the false detection rate (type I error rate) of such procedures may lead to excessively stringent acceptance criteria. In the recent physics literature, two promising statistical tools have been proposed to overcome these limitations. In 2005, a method to "find needles in haystacks" was introduced by Pilla et al. [1], and a second method was later proposed by Gross and Vitells [2] in the context of the "look elsewhere effect" and trial factors. We show that, for relatively small sample sizes, the former leads to an artificial inflation of statistical power that stems from an increase in the false detection rate, whereas the two methods exhibit similar performance for large sample sizes. Finally, we provide general guidelines to select between statistical procedures for signal detection with respect to the specifics of the physics problem under investigation.

Keywords: signal detection, global p-value, look-elsewhere effect.

1 Introduction

In High Energy Physics (HEP) the statistical evidence for new physics is determined using p-values, i.e., the probability of observing a signal as strong or stronger than the one observed if there had been no underlying posited reso-

nance. If the location of the resonance in question is known, the p-value can be easily obtained with classical methods such as the Likelihood Ratio Test (LRT), using the asymptotic distribution provided under the conditions specified in Wilks or Chernoff's theorems [3, 4]. Unfortunately, the most realistic scenario involves signals with unknown locations, leading to what is known in the statistics literature as a non-identifiability problem [5].

To tackle this difficulty, physicists traditionally considered multiple hypothesis testing: they split the range of the energy spectrum¹ into a predetermined number of bins, and sequentially test for resonance in each bin location [6, 7]. As discussed in detail in Section 3, when the number of bins is large, the detection threshold for the resulting *local* p-values becomes more anti-conservative than the overall significance, which translates into a higher number of false discoveries than expected. We discuss the details of this phenomenon in Sections 2 and 3. The situation is particularly problematic in the more realistic case of dependent tests. These occur for instance when the signal is dispersed over several energy bins and thus its detection in a particular bin may be correlated with that in nearby bins. Unlike the case of independent tests in which the local significances can be determined exactly, in presence of dependence, we can only determine upper bounds for these significances, such as those provided by the Bonferroni's correction. Unfortunately, such bounds may be excessively conservative [8, 9]. We focus on the problem of finding a single peak above background rather than multiple signals, and thus appealing methods such as Tukey's multiple comparisons [10] or the popular False Discovery Rate (FDR) [11–13] do not apply in this scenario.

^ae-mail: s.algeri14@imperial.ac.uk

^be-mail: d.van-dyk@imperial.ac.uk

^ce-mail: conrad@fysik.su.se

^de-mail: brandon.anderson@fysik.su.se

¹The search of a new source emission can occur over the spectrum of the mass, energy or any other physical characteristic; for simplicity, we will refer to it as energy spectrum.

In order to overcome some of the limitations arising in multiple testing, two promising methods have been recently proposed in physics literature. The first (henceforth PL) was introduced in 2005 [1] and refined in [14]. Its methodology relies on the Score function and is purported to be more powerful than the usual Likelihood Ratio Test (LRT) approach. Unfortunately, the mathematical implementation of the method is not straightforward, which strongly limited its diffusion within the physics community. The second approach (hereinafter GV) belongs to the class of LRT-based methods. It was first introduced in 2010 [2], and recently extended [15] to compare non-nested models. In contrast to PL, GV enjoys easy implementation, which has led to a wide range of applications in various searches for new physics including in the discovery of the Higgs boson [6, 7, 16, 17]. From a theoretical perspective, both approaches require an approximation of tail probabilities of the form $P(\sup Y_t > c)$, where Y_t is either a χ^2 or a Gaussian process. As described in Section 4, the main difference between the two solutions is that GV formalizes the problem in terms of up-crossings of a stochastic process, whereas PL provides an approximation based on tube formulae. Instead of focusing on the mathematical details of the methods, we emphasize their computational implementation; readers are directed to [1, 2, 14, 15, 18–20] for technical development.

While either GV or PL can be used to control the false detection rate and ensure sufficient statistical power, they can be computationally expensive in complex models. Multiple hypothesis testing procedures, on the other hand, can be much quicker, but may be overly conservative in terms of the false detection rate. In order to optimize computational speed while maintaining the statistical properties of GV and/or PL, we propose a simple *combined approach* that select among the procedures.

The remainder of this paper is organized as follows: in Section 2 we review the background of hypothesis testing, we define the auxiliary concepts of *goodness* of a test and *local power*, which are used for our comparison of PL and GV. In Section 3, we review the multiple testing approach for signal detection and we underline the respective disadvantages in terms of significance requirements. In Section 4, we provide a simplified overview of the technical results of PL and GV. In Section 5, a suite of simulation studies is used to highlight the performance of the two methods in terms of approximation to the tail probabilities, false detection rate and statistical power. We show that both solutions exhibit advantages and suffer limitations, not only in terms of computational requirements and statistical power, but most importantly, in terms of the specific conditions they require of the models being tested. An application to a realistic data simulation is conducted in Section 6. The combined approach is proposed in Section 7 and discussion in Section 8.

2 Type I error, local power and good tests of hypothesis

Consider the framework of a classical detection problem. Suppose N event counts are observed over a predetermined energy band \mathcal{Y} . We are interested in knowing if some of these events are due to a new emission source or if they all can be attributable to the background and its random fluctuations. We further assume that if there is no new source, the energy y of the N events can be modeled using a probability density function (pdf) $f(y, \phi)$ over \mathcal{Y} where ϕ is a potentially unknown free parameter. Whereas, if the new resonance is present, events associated with it have energy distribution $g(y, \theta)$ over \mathcal{Y} , and we let $\theta \in \Theta$ with Θ representing the search window for the new resonance over the energy range. Typically $\Theta \equiv \mathcal{Y}$, but in principle one could consider $\Theta \subset \mathcal{Y}$. Thus, we can write the full model for N counts as

$$(1 - \eta)f(y, \phi) + \eta g(y, \theta), \quad (1)$$

where η is the source strength, and positive values of η indicate the presence of the new signal.

From a statistical perspective, the search for new physics corresponds to a test of hypothesis in which the *null hypothesis*, H_0 , which stipulates that only background counts are observed, is tested against the *alternative hypothesis*, H_1 , which stipulates a proportion η of the observed counts are due to new physics. Notationally this test is written

$$H_0 : \eta = 0 \quad \text{versus} \quad H_1 : \eta > 0. \quad (2)$$

The test is then conducted by specifying an opportune test statistic T , whose observed value t_{obs} is calculated on the available data, and a detection is claimed if t_{obs} exceeds a specified detection threshold t_α . The latter is determined by controlling the probability of a *type I error* or the false detection rate, which we allow to be no larger than a pre-determined level α . For obvious reasons, it is sensible to choose α sufficiently small, and it is common practice in physics to adopt a 3, 4 or 5 σ thresholds i.e.,

$$\alpha = 1 - \Phi(x) \quad x = 3, 4, 5, \quad (3)$$

where $\Phi(\cdot)$ is the cumulative density function (cdf) of a standard normal distribution. If $t_{obs} > t_\alpha$ a discovery is claimed, whereas if $t_{obs} \leq t_\alpha$ we conclude that there is no sufficient evidence to claim detection of a new signal.

An equivalent formulation of a test of hypothesis can be made in terms of a *p-value* i.e., the probability of observing a value of T that, under the hypothesis of no signal emission (H_0), is greater than t_{obs} . Formally

$$\text{p-value} = P(T \geq t_{obs} | \eta = 0). \quad (4)$$

The p-value is then compared to the target probability of a type I error, α . In this case, a discovery is claimed if p-value $< \alpha$, whereas the new resonance is not detected if p-value $\geq \alpha$.

In addition to the type I error, another important property of a test of hypothesis is its statistical *power* i.e., the probability of detecting the new signal when it is present. For the test in (2) we can write

$$\begin{aligned} \alpha &= P(T > t_\alpha | \eta = 0) \\ \text{Power}(\eta, \theta) &= P(T > t_\alpha | \eta, \theta), \quad \eta > 0. \end{aligned} \quad (5)$$

The goal is to construct a *good* detection test, that is, a test with the probability of false detection, equal to or smaller than the pre-determined level α , but with the power as large as possible.

Consequently, if two or more tests with the same level α are to be compared, the test with higher power is preferred. As specified in (5), for the model in (1) the power depends on both the signal strength η and its location θ . For η , the detection power can be summarized using *upper limits* as discussed in [21], whereas in this paper, we focus on the power with respect to the source location. This is of particular importance when the dispersion of the signal depends on its position (as in our examples in Section 5), and widely spread source signals are expected to be more difficult to detect, i.e., exhibit lower statistical power. Hereafter, we refer to the power at a fixed location θ as the *local power*, and we say that a test is *uniformly more powerful locally* than another test with the same level α , if, for fixed η , its local power is greater than or equal to that of the other test, for every possible θ in the energy range Θ . We investigate the *goodness* and the local power of PL and GV in Section 4.

Typically, the exact distribution of the test statistic T cannot be specified explicitly, and classical statistical methods rely on its asymptotic distribution. It follows that the resulting p-values, α , and power are also asymptotic quantities. In this paper, we mainly consider the asymptotic distributions of various test statistics and thus, the p-values, α levels and powers that we quote are implicitly asymptotic quantities. The only exceptions are the values quoted in the simulation studies in Section 5. There, the distribution of reference is the simulated distribution of T , and we refer to the quantities of interest as simulated false detection rate and simulated power.

3 Signal detection via multiple hypothesis testing

As anticipated in Section 1, the statistical detection of new physics can often be viewed as a multiple hypothesis testing problem. An ensemble of R tests are conducted simultaneously, any of which can result in a false detection. While the individual tests are designed to control their specific false detection rate, the overall probability of having at least one

false detection increases as R increases, leading to a higher rate of false discoveries than expected.

For the test in (2), a natural choice of the test statistic T is the LRT. Define

$$LRT_\theta = -2 \log \frac{L(0, \hat{\phi}_0, -)}{L(\hat{\eta}_1, \hat{\phi}_1, \theta)}, \quad (6)$$

where $L(\eta, \phi, \theta)$ is the likelihood function under (1). Notice that under H_0 (i.e., $\eta = 0$), the parameter θ has no meaning and no value. The numerator and denominator of (6) are the maximum likelihood achievable under H_0 and H_1 respectively, with $\hat{\phi}_0$ being the Maximum Likelihood Estimate (MLE) of ϕ under H_0 and $\hat{\phi}_1$ and $\hat{\eta}_1$ the MLEs under H_1 . Under H_0 , the distribution of the data does not depend on θ . Because this violates a key assumption of both Wilks or Chernoff's theorems [3, 4], the distribution of LRT is not known and we cannot directly compute the p-value for (2).

To overcome this difficulty, a naïve approach involves the discretization of the energy range Θ into R bins or search regions, resulting in a grid of fixed values $\Theta_G = \{\theta_1, \dots, \theta_R\}$, where θ_r is typically the center of bin r . R simultaneous LRTs are then conducted for the hypotheses in (2), fixing θ in (6) to be equal to each of the $\theta_r \in \Theta_G$. In this way, a set of R local p-values is produced, and the smallest, namely p_L , is compared with the established target probability of type I error, α_L . Notice that α_L corresponds to the false detection rate for a specific test among the R available, and thus is the local significance. However, we must take account of the fact that R hypotheses are being tested simultaneously and must also consider the chance of having at least one false detection among the ensemble of R tests, namely the global significance, α_G .

If the R tests are independent, i.e., detecting a signal in a given energy bin does not depend on its detection in other bins, it can be easily shown [8] that

$$\alpha_G = 1 - (1 - \alpha_L)^R, \quad (7)$$

and the resulting adjusted (global) p-value [8, 9] is

$$p_G = 1 - (1 - p_L)^R. \quad (8)$$

Consider a toy example in which we have, 50 energy bins and 50 independent tests at the 5σ significance level, the chance of having at least one false detection among the 50 tests, i.e., the overall false detection rate, is $\alpha_G = 1.4 \cdot 10^{-5}$ which corresponds to 4.18σ significance. This is approximately 50 times larger than the $\alpha_L = 2.87 \cdot 10^{-7}$ associated with 5σ . Conversely, if the R tests are dependent, as in the case of disperse source emission, controlling for the false detection rate is more problematic. In this scenario, contrary to (7), an exact general relationship between α_L and α_G cannot be established, since the specific dependence structure varies on a case-by-case basis. Thus, the only general state-

ment that we can make is

$$\alpha_G \leq R\alpha_L. \quad (9)$$

The adjusted p-value corresponding to (9) is known as the Bonferroni correction [8], specifically,

$$p_{BF} = Rp_L \quad (10)$$

which bounds p_G in that $p_G \leq p_{BF}$. In particular, p_{BF} is a first order approximation of p_G , and thus the two p-values are equivalent when dealing with strong signals, i.e., when $p_L \rightarrow 0$. This is reflected in the toy example above, where p_{BF} is equal to p_G , and also leads to 4.18σ significance. (Recall $\frac{\alpha_G}{\alpha_L} \approx 50$ in the toy example.)

Despite their easy implementation, these procedures are often dismissed by practitioners because, in addition to the stringent requirements to control for the overall false detection rate, they artificially depend on the number of energy bins R . This aspect is particularly troublesome given the typically arbitrary nature of setting R when discretizing the energy spectrum Θ .

4 Needles in haystacks and look elsewhere effect

Although the multiple hypothesis testing strategy introduced in Section 3 may be used in the search of new physics to overcome the problem of parameters which are present only under H_1 , recent developments in both the statistics and physics literatures tackled this issue in a different way. They consider a single test of hypothesis and a unique global p-value. The key element of these methods is to consider new test statistics, which are not affected by the non-identifiability of the parameters. The two methods we consider follow a similar overall strategy which we now summarize.

Consider the model in (1). We denote the MLE of the parameters η and ϕ by $\hat{\phi}_\theta, \hat{\eta}_\theta$ for each fixed value $\theta \in \Theta$, and we specify a *local* test statistic $C(y, \hat{\phi}_\theta, \hat{\eta}_\theta, \theta)$ for the test in (2). For brevity, we write $C(y, \hat{\phi}_\theta, \hat{\eta}_\theta, \theta)$ as $C(\theta)$. In practice, for each fixed value $\theta_r \in \Theta_G$, we compute $c(\theta_1), \dots, c(\theta_R)$, where $c(\theta_r)$ corresponds to the observed value of $C(\theta)$ with $\theta = \theta_r$. The collection of values $\{c(\theta_1), \dots, c(\theta_R)\}$ can be viewed as a realization of a stochastic process $\{C(\theta), \theta \in \Theta\}$, and a *global* test statistic, for (2) is

$$C = \sup_{\theta \in \Theta} C(\theta). \quad (11)$$

Because we only observe $C(\theta)$ for $\theta_r \in \Theta_G$, the observed value of C is

$$c(\hat{\theta}) = \max_{\theta_r \in \Theta_G} c(\theta_r) \quad (12)$$

where $\hat{\theta}$ is the value $\theta_r \in \Theta_G$ where this maximum is attained, and which corresponds to our estimate of the signal

location. Finally, the *global* p-value of the test is obtained by approximating the tail probability

$$P(C > c(\hat{\theta})) \quad (13)$$

under H_0 . The choice of the statistic C and the approximation method for computing (13) are the main characteristics differentiating the approaches of PL and GV.

To derive C , PL [1, 14] considers the Score process $\{C_{PL}^*(\theta), \theta \in \Theta\}$, with

$$C_{PL}^*(\theta) = \sum_{i=1}^N \left[\frac{f(y_i, \phi)}{g(y_i, \theta)} - 1 \right]$$

being the Score function of (1) under H_0 and the generic local statistic $C(\theta)$ above is replaced by the normalized Score function,

$$C_{PL}(\theta) = \frac{C_{PL}^*(\theta)}{\sqrt{NW(\theta, \theta)}}. \quad (14)$$

$W(\theta, \theta^\dagger)$ is the covariance function of $\{C_{PL}^*(\theta), \theta \in \Theta\}$. The structure of $W(\theta, \theta)$ depends on whether the free parameter under H_0 , ϕ , is known or not [1, 14] and $\{C_{PL}(\theta), \theta \in \Theta\}$ is the stochastic process of interest. We let $C_{PL} = \sup_{\theta \in \Theta} C_{PL}(\theta)$ and $c_{PL}(\hat{\theta})$ be its observed value. In order to simplify notation we drop the dependence on $\hat{\theta}$ of the latter and hereafter refer to it with c_{PL} . The corresponding global p-value is $P(C_{PL} > c_{PL})$; [14] prove that, under H_0 , C_{PL} converges to the supremum of a mean zero Gaussian process as $N \rightarrow \infty$. The approximation, p_{PL} , of $P(C_{PL} > c_{PL})$ is obtained through so-called tube formulae for Gaussian processes [20]. If θ is one-dimensional and as $c_{PL} \rightarrow \infty$,

$$p_{PL} = \frac{\xi_0}{2\pi} P(\chi_2^2 \geq c_{PL}^2) + \frac{1}{2} P(\chi_1^2 \geq c_{PL}^2), \quad (15)$$

where ξ_0 is a geometric constant depending on the covariance function $W(\theta, \theta^\dagger)$ and typically computed via numeric integration [1, 14]. When ϕ is unknown, its value is replaced with its MLE $\hat{\phi}_0$ under H_0 and the covariance function $W(\theta, \theta^\dagger)$ is modified accordingly.

Instead of the Score function, GV in [2] focuses on the LRT in (6), and thus $C_{GV}(\theta) = LRT(\theta)$. For the specific case of (2), H_0 is on the boundary of the parameter space, and thus under H_0 the LRT process converges asymptotically to a $\frac{1}{2}\chi_1^2 + \frac{1}{2}\delta(0)$ random process [2, 15]. With this choice, and again, dropping the dependence on $\hat{\theta}$, we let $C_{GV} = \sup_{\theta \in \Theta} C_{GV}(\theta)$ and c_{GV} be its observed value depending on the data. The global p-value $P(C_{GV} > c_{GV})$, is approximated by p_{GV} in (16) as $c_{GV} \rightarrow \infty$

$$p_{GV} = \frac{P(\chi_1^2 > c_{GV})}{2} + E[U(c_0)|H_0]e^{-\frac{c_{GV}-c_0}{2}}. \quad (16)$$

The main quantity in (16) is the expected number of up-crossings, $U(c_0)$, of the LRT process from below to above

a threshold $c_0 \ll c_{\text{GV}}$, under H_0 . The expected number $E[U(c_0)|H_0]$ is obtained via Monte Carlo simulation, whereas c_0 is chosen to be small enough so that a reliable estimate of $E[U(c_0)|H_0]$ can be obtained with a small Monte Carlo simulation size, but large enough so that the effect of the resolution R of Θ_G on the number of upcrossings is negligible (see [2]). Although (15) and (16) both hold when c_{PL} and c_{GV} are large, when they are small, the right hand sides of (15) and (16) provide upper bounds for the respective tail probabilities.

GV's global p-value, p_{GV} , is always greater than or equal to the smallest local p-value, p_{L} , introduced in Section 3. Thus GV always leads to an equal or smaller number of false discoveries than one would have using multiple hypothesis testing. This can be easily shown by noticing that for the test in (2)

$$p_{\text{L}} = \frac{1}{2}P(\chi_1^2 > LRT_{\theta^*}) \quad (17)$$

where LRT_{θ^*} is calculated according to (6) with $\theta = \theta^*$. Notice that $\theta^* \equiv \hat{\theta}$, i.e., the location where the smallest p-value is observed is also where the observed local LRT statistic, achieves its maximum. Thus, the LRT_{θ^*} coincides with the observed value c_{GV} of the GV test statistic C_{GV} . It follows by (16) and (17) that the inequality $p_{\text{GV}} \geq p_{\text{L}}$ always holds.

Another fundamental difference between the multiple hypothesis testing approach in Section 3 and the methods discussed in this section is the level at which the optimization occurs. In the former, the p_{L} is the minimum of set of local p-values

$$p_{\text{L}} = \min_{\theta_r \in \Theta_G} p(\theta_r),$$

and the result, is eventually corrected afterwards according to (8) or (10). Conversely, as expressed in (12) in PL and GV, the optimization occurs with respect to the statistic $C(\theta)$, and a correction for p_{L} is eventually generated intrinsically, by approximating the tail probability of the test statistic C .

5 Simulation studies

A fundamental result in probability theory states that the Score test and the LRT are asymptotically equivalent (i.e., for large sample sizes). As shown in [1], the same can be proven for the C_{PL} and C_{GV} of PL and GV, respectively. However, this theoretical result is not necessarily reflected in practice when dealing with limited sample sizes.

In order to further investigate this, we consider two examples. In Example I, we refer to the toy model in [1] where a Breit-Wigner resonance is superimposed on a linear background. The full model is

$$(1 - \eta) \frac{1 + 0.3y}{2.6} + \eta \frac{0.1}{k_\gamma \pi (0.01 + (y - \gamma)^2)} \quad (18)$$

where k_γ is a normalizing constant, $y \in [0; 2]$ and $\gamma \in (0; 2]$. Notice that the null model has no free parameters and thus PL can be directly applied with no further adjustment of the covariance function (see Section 4). In Example II, the background is power-law distributed with unknown parameter τ . The signal component is modeled as a Gaussian bump with dispersion proportional to the signal location. Specifically, the full model is

$$(1 - \eta) \frac{1}{k_\tau y^{\tau+1}} + \frac{\eta}{k_{M_\chi}} \exp\left\{-\frac{(y - M_\chi)^2}{0.02M_\chi^2}\right\} \quad (19)$$

with k_τ and k_{M_χ} normalizing constants, $y \in [1; 10]$, $\tau > 0$ and $M_\chi \in [1; 10]$. Owing to the unknown parameter τ under H_0 , we must use the extended theory in [14] for PL. The pdfs used in Example I and II are plotted in Fig. 1.

For both examples, we evaluate the false detection rate (or type I error), and the local power as described in Section 2, with sample sizes of 10, 50, 100, 200 and 500. The false detection rate and local power are obtained via Monte Carlo simulations from the null model ($\eta = 0$) and from the alternative model with $\eta = 0.2$, respectively. Although τ is unknown in Example II, it can be estimated with the MLE $\hat{\tau}$ under H_0 . The simulations are then drawn from (19) with $\tau = \hat{\tau}$. This simulation procedure is known in the statistical literature as the parametric bootstrap [22]. In principle, the observed sample used to compute $\hat{\tau}$ could either come from the null or from the alternative model. Thus, in order to evaluate the consistency of PL and GV in both situations, two further sub-cases are needed. In Example IIa, we draw the "observed" sample from (19) with $\eta = 0$ and $\tau = 1.4$, i.e., in absence of new physics. In Example IIb, we draw the "observed" sample with $\eta = 0.2$, $\tau = 1.4$ and $M_\chi = 9$.

Results of the simulation studies appear in Fig. 2. Its columns correspond to Example I, Example IIa and Example IIb, respectively. In the first row, we report the simulated detection rates; the simulated test statistics C_{PL} and C_{GV} (where θ is either γ or M_χ) were calculated for each of 100,000 datasets generated from the null model. These values were then compared to the nominal thresholds at 3σ , obtained, as in (20) and (21), by setting p_{PL} and p_{GV} in (15) and (16) equal to 0.997 and solving for c_{PL} and c_{GV} respectively, i.e.,

$$0.997 = \frac{\xi_0}{2\pi} P(\chi_2^2 \geq c_{\text{PL}}^2) + \frac{1}{2} P(\chi_1^2 \geq c_{\text{PL}}^2) \quad (20)$$

$$0.997 = \frac{P(\chi_1^2 > c_{\text{GV}})}{2} + E[U(c_0)|H_0] e^{-\frac{c_{\text{GV}} - c_0}{2}}. \quad (21)$$

In the second row of Fig. 2, we plot the local power functions; the procedure is the same as for the simulated false detection rates except the 100,000 datasets were generated from the alternative models with $\eta = 0.2$ with different values for the location parameters γ and M_χ . In the third row,

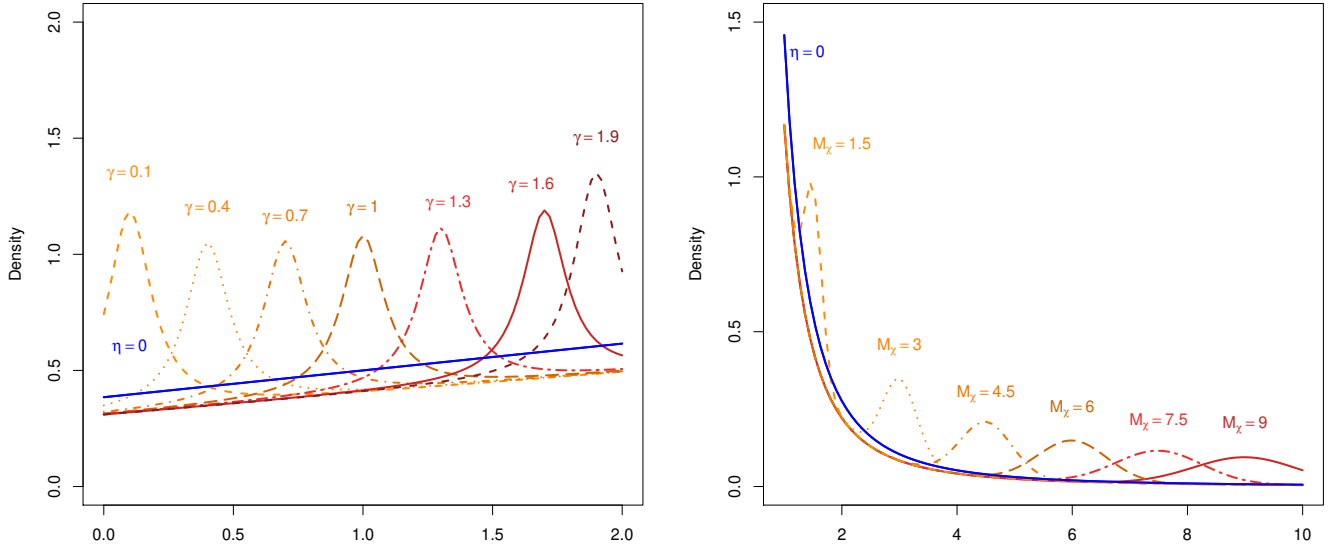


Fig. 1 Left panel: probability density functions for Example I under H_0 (blue line) and H_1 (orange lines) with $\eta = 0.2$ and $\gamma = 0.1, 0.4, 0.7, 1, 1.3, 1.6, 1.9$. Right panel: probability density functions for Example II under H_0 (blue line) with $\tau = 1.4$ and H_1 (orange lines) with $\eta = 0.2$ and $M_\chi = 1.5, 3, 4.5, 6, 7.5, 9$.

we evaluate an adjusted version of the local power; the simulated values of C_{PL} and C_{GV} are the same as used in the plots in the second row, but instead of comparing them with the nominal thresholds c_{PL} and c_{GV} , we compared them with their empirical (bootstrap) thresholds. The empirical threshold correspond to the 0.997 quantiles of the 100,000 simulated values of C_{PL} and C_{GV} generated for the first row of Fig. 2, i.e., the empirical distributions of the test statistic under H_0 . Looking at the first row of Fig. 2, the simulated false detection rates associated with GV are always consistent with the nominal 3σ error rate. This is not the case for PL. Although the false detection curves appear to approach the desired value as the sample size increases, they are always higher than expected. Looking at the second row of Fig. 2, on the other hand, the simulated local power of PL is always higher than that of GV, at least for the smaller sample sizes. The difference between the local power functions decreases when the sample size increases, leading to two identical curves at 500 counts. These results are, however, not sufficient to determine whether PL or GV is better. In particular, we recall our definition of *good* test as a test of hypothesis which makes the power as high as possible while keeping the false detection rate less than or equal to α_G , which in our examples is set to 0.003. In this sense, the increased power of PL is artificial; it is due to an increase of the probability of a type I error, and thus does not satisfy our *goodness* requirements. Conversely, GV seems to fit in our definition of a good test of hypothesis: the false detection rate is equal to or smaller than expected, and its local

power function approaches that of PL as the sample size increases. Notice that as described in [1], the error rate of p_{PL} as an approximation to $P(C_{PL}(\hat{\theta}) > c_{PL})$ is in the order of $o(c^{-1}e^{-c^2/2})$. In our three examples the values for c_{PL} solving (20) are 13.580, 13.408 and 13.768 respectively, leading to an approximation error of the order of 10^{-38} . Thus, the high false detection rate of PL is unlikely to be due to an underestimation of the 3σ nominal thresholds.

A more detailed comparison of the detection power of PL and GV can be done by correcting the false detection rate (as in the third row of Fig. 2). Specifically, we can use the empirical detection threshold when evaluating the local power of the two procedures. This guarantees a false detection rate of 0.003 (3σ significance). GV has a lower chance of Type I error than the adjusted PL, i.e., the adjusted PL has probability 0.003 of Type I error, which bounds that of GV, see first row of Fig. 2. Despite this, for all three examples and for all signal locations (values of γ or M_χ) considered, GV is equally or more powerful than PL when using the empirical threshold. Thus, the evidence from this simulation indicates that for small sample sizes, GV is uniformly locally more powerful than PL.

Comparing the local power functions in the second and third rows of Fig. 2 with the pdfs in Fig. 1, we see that, for Example I, the detection power of the testing procedures is affected by both the specific location of the signal and its dispersion. The power is higher when a weakly disperse resonance is located in a low background region. In Example II, only the location of the source emission seems

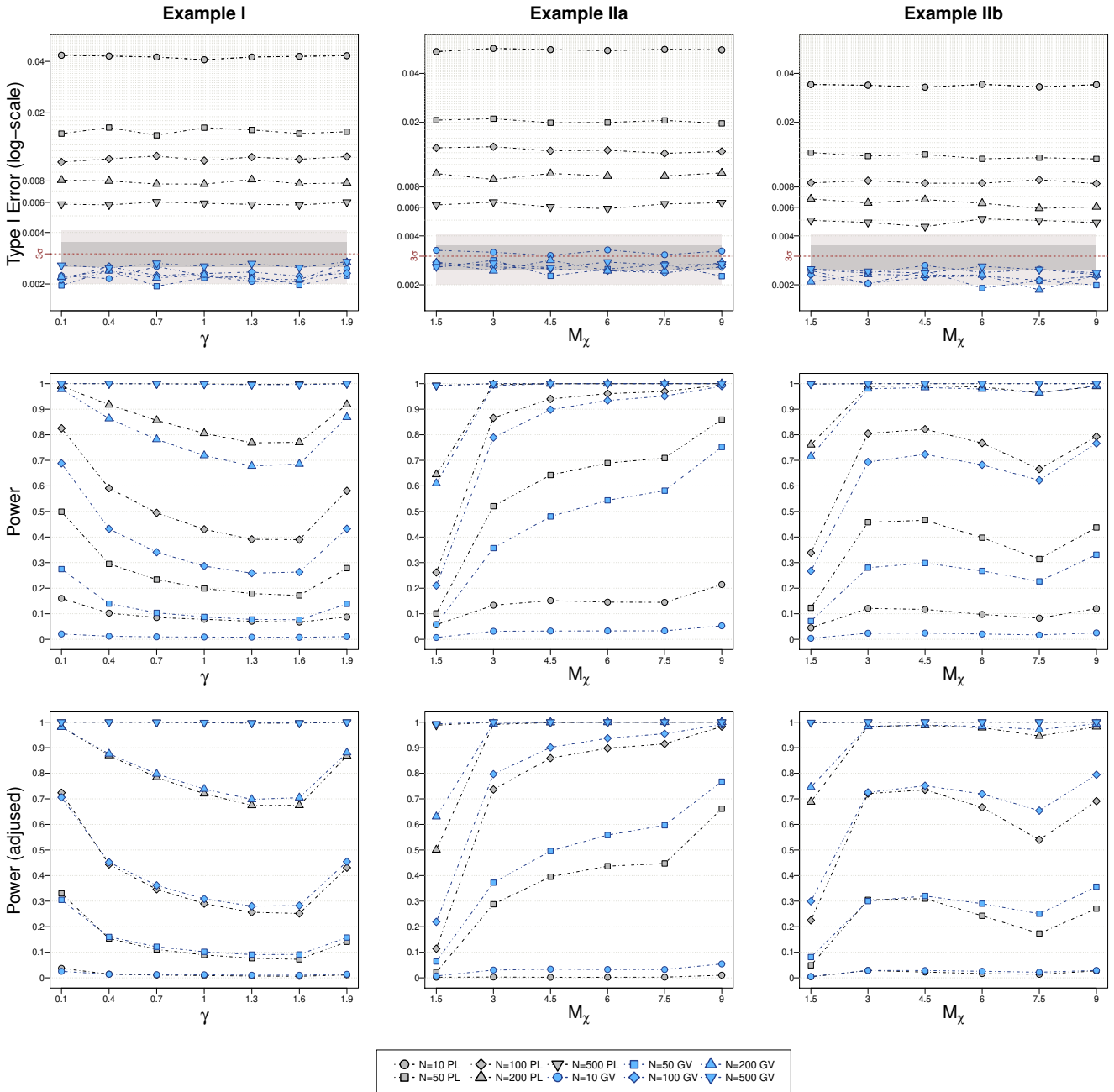


Fig. 2 Simulated probability of type I error (top row), power (middle row) and adjusted power (bottom row) for Example I (first column), Example IIa (second column) and Example IIb (third column) with different sample size N over 100,000 simulations. The gray symbols corresponds to PL and the blue symbols to GV. Shaded areas indicate regions expected to contain 68% (dark gray) and 95% (light gray) of the symbols if the nominal type I error of 0.003 holds.

to affect the power. In particular, detection appears to be more difficult in high background areas of the spectrum, and thus the strength of the signal is weaker with respect to the background sources. These issues are overcome if at least 500 counts are available; in this case both procedure exhibit maximum detection power regardless the location or dispersion of the signal.

Few computational difficulties arose when implementing PL and GV. In PL the most problematic step is the calculation of the geometric constant ξ_0 in (15). Numerical methods are often required for the computation of the necessary nested integrals; this can significantly slow down the testing procedure when dealing with complicated models. For the specific case of Examples I and II, small ranges over the

Method	Signal Location	Signal Strength	Sig.
Unadjusted local	35.82	0.042	5.920σ
Bonferroni adj. local	35.82	0.042	5.152σ
Gross & Vitells	35.82	0.042	5.192σ
Pilla et al.	35.82	0.042^*	5.531σ

*Obtained afterwards via MLE by fixing the signal location to its PL estimate (see text).

Table 1 Summary of multiple hypothesis testing, GV and PL on the Fermi LAT simulation. For the multiple hypothesis testing case, the smallest of $R = 80$ (undadjusted local) p-values, its Bonferroni adjusted version, along with GV and PL, are reported with their respective statistic.

energy spectra \mathcal{Y} ($[0; 2]$ and $[1; 10]$ respectively) were chosen in order to speed up the computation of these integrals, which tended to diverge quite easily when considering larger energy bands. If nuisance parameters are present under the null model, such as τ in Example II, the calculation of ξ_0 is more complicated than simply plugging in the MLE of these parameters. Instead, a new more complex covariance function must be used (see [14] for more details).

The main difficulty with GV is the multidimensional constrained optimization that must be repeated over the grid Θ_G of size R for each simulated dataset (R is set to 50 in both Example I and II). However, if the nuisance parameter under H_1 , θ , is one-dimensional, the necessary computation can easily be accomplished by choosing a small threshold c_0 as described in Section 4 and in more detail in [2]. The discussion of the multidimensional case is postponed to Section 8.

6 Application to realistic data

As a practical application, we perform the testing procedures discussed in Section 3 and 4 on a simulated observation of a monochromatic feature by the Fermi Large Area Telescope (LAT). The existence of such a feature within the LAT energy window would be an indication of new physics; of particular interest, it could result from the self-annihilation of a dark matter particle, and has consequently been the subject of several recent studies [24–26]. We consider emission resulting from the self-annihilation of a particle making up the substantial dark matter mass of the Virgo galaxy cluster (distributed according to [27]). We further specify that the particle have a mass of 35 GeV and a direct-to-photon thermally-averaged annihilation cross section of $1 \times 10^{-23} \text{ cm}^2$. Competing with this signal, we introduce a simple astrophysical background corresponding to isotropic emission following a spectral power-law with index 2.4, i.e., $\tau = 1.4$. Both signal and background models are then simulated for a five-year

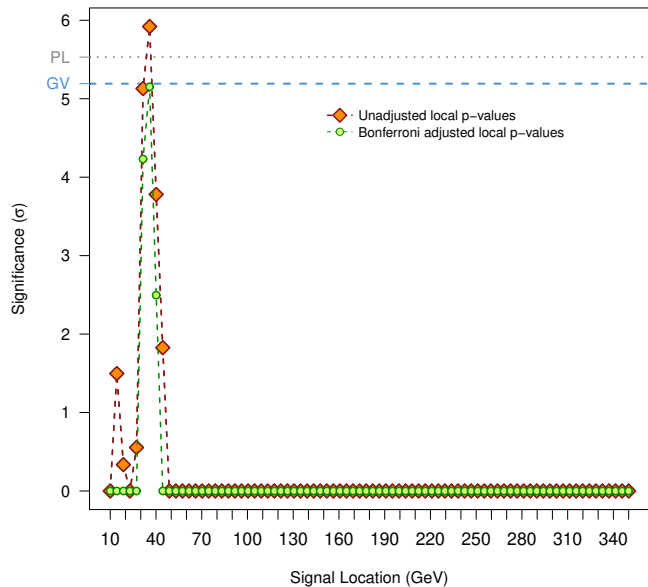


Fig. 3 Unadjusted local p-values (orange diamonds), Bonferroni adjusted local p-values (green dots), PL global p-value (gray dotted line) and GV global p-value (blue dashed line) for the Fermi LAT simulation. The Bonferroni adjusted local p-value is only slightly more conservative than the GV p-value

observation period using the *gtobssim* package, available at <http://fermi.gsfc.nasa.gov/ssc/data/analysis/software>, which takes into account details of the instrument and orbit. We bin the photons registering within 1 degree of the source into 80 energy bins, spaced equally from 10–350 GeV. The setup yields, on average, 64 signal and 2391 background events.

The full model is the same as in Example II i.e., as given in (19); results of the several methods are shown in Table 1 and Fig. 3. In the multiple hypothesis testing analysis, the smallest of the local p-values is reported along with the respective estimates for the signal strength and location. As discussed in Section 4, the latter are equivalent to those obtained with GV. The test statistic of PL, $C_{PL}(\hat{\theta})$, is constructed under the assumption that $\eta = 0$, and thus does not depend on the signal strength. However, it does depend on the location of the source emission, and thus the estimation of η under H_1 must be conducted once the signal location has been estimated (through MLE for instance). In our analysis, the PL estimate for the source location is equivalent to both that of GV and of the local p-values methods; it follows that the resulting MLE for the signal strength is the same for all methods.

The local p-value approach leads to the largest significance of 5.920σ , followed by PL 5.531σ , GV 5.192σ and finally Bonferroni with 5.152σ . Although PL provides the most significant of the global p-values, it is difficult to interpret this result given PL's higher than expected rate of false detections in the simulation study. The Bonferroni adjusted

	Unadjusted local	Bonferroni adj. local	Gross & Vitells
Bkg only	97056	37	2907
Time (secs)	0.974	0.000	136.282
Bkg+sig	10496	45210	44294
Time (secs)	1.061	0.000	137.532

Table 2 Summary on the analysis of 100,000 simulated datasets from Example II in Section 5. We report the number of times each testing method is used by the combined approach to make a final decision at 3σ , and the respective average computational times. The first two lines refer to the background only simulations and whereas the last two lines correspond to the background + signal simulations.

local p-value, over the set of 80 simultaneous tests, it is only slightly more conservative than GV. The disparity between the two is expected to grow, however, as the number of bins over the energy spectrum increases.

7 A combined approach

On the basis of the results of the previous sections, it is possible to establish general guidelines for selecting the appropriate statistical testing procedure. The goal is to guarantee adequate statistical properties, while minimizing computational effort. This can be accomplished by combining the simplicity of multiple hypothesis testing with the robustness of global p-values in a multi-stage procedure. Specifically, Fig. 4 summarizes a simple step-by-step algorithm where multiple hypothesis testing methods are implemented first, and the more time-consuming GV and PL are implemented only if simple methods exhibit poor type I error rates and/or power.

We focus on the case of a one-dimensional search. In which case,

$$p_L \leq p_{PL} \approx p_{GV} \lesssim p_{BF}, \quad (22)$$

where the approximation sign in the last inequality covers for the atypical, but possible, situation where $p_{GV} \geq p_{BF}$. Despite this possibility, the bound in (22) is an approximation for large R . Specifically, combining (16) and (17),

$$p_{GV} = p_L + E[U(c)|H_0] \leq p_L + p_{BF} = (R+1)p_L. \quad (23)$$

Where $E[U(c_{GV})|H_0] = E[U(c_0)|H_0]e^{-\frac{c_{GV}-c_0}{2}}$ is the expected number of upcrossings of the observed value for the test statistic c_{GV} , i.e., $c_{GV} = LRT_{\theta^*}$ in (17). Since the expected of upcrossings above c_{GV} is bounded by the expected number of times the LRT process takes a value greater than c_{GV} , i.e., $Rp_L = p_{BF}$, we have

$$p_{GV} \leq \frac{R+1}{R} p_{BF} \approx p_{BF} \quad \text{for large } R. \quad (24)$$

	Type I error	Power
Unadjusted local	0.03033	0.89502
Bonferroni adj. local	0.00040	0.45211
Gross & Vitells	0.00089	0.53159
Combined approach	0.00087	0.53161

Table 3 Probability of type I error and power of the testing methods and combined approach implemented on 100,000 simulated datasets from Example II in Section 5.

A more formal justification of (23 and 24) can be found in [28].

In order to implement the combined approach, we first calculate the R unadjusted local p-values over the grid Θ_G ; the minimum of these p-values is denoted by p_L . From (22), if we observe $p_L > \alpha_G$ we fail to reject H_0 with any of the procedures and we can immediately conclude that we cannot reject H_0 . On the other hand, if $p_L \leq \alpha_G$, a correction for the simultaneous R tests is needed, and because of its easy implementation, we compute p_{BF} . Whereas, if $p_{BF} < \alpha_G$, then all methods reject H_0 , and we can claim evidence in favor of the new source. Conversely, if $p_{BF} \geq \alpha_G$ we should implement a method that is typically less conservative than Bonferroni's correction, when dealing with large significances (e.g. $3\sigma, 4\sigma, 5\sigma$), such as GV or PL. Specifically, on the basis of the simulations in Section 5, GV appears to be preferable for small sample sizes, as it provides a false positive rate less than or equal to α_G . For large sample sizes, PL and GV are equivalent, and the decision between GV and PL depends on the details of the models compared. As discussed in Section 5, PL requires extensive numerical integration which can diverge for large search windows Θ , while GV requires a small number of Monte Carlo simulations which might become troublesome for complicated models. Finally, if $p_{GV} < \alpha_G$ (or $p_{PL} < \alpha_G$) we can claim evidence in support of the new resonance, whereas if $p_{GV} \geq \alpha_G$ (or $p_{PL} \geq \alpha_G$) we cannot claim that a signal has been detected.

The combined approach involves choosing a procedure based on the characteristics of the data. Thus, one might be concerned about possible "flip-flopping" similar to that described by Feldman and Cousins in [29] in the context of confidence intervals. As argued below, however, this is not the case for the combined approach illustrated in Fig. 4. By virtue of (22), both the type I error and the power of the combined approach are approximately equivalent to those of GV (or PL) for large values of R . For clarity, we hereinafter suppose GV is used rather than PL in the combined approach. The statistical results follow in exactly the same way however, if PL is used for large sample sizes.

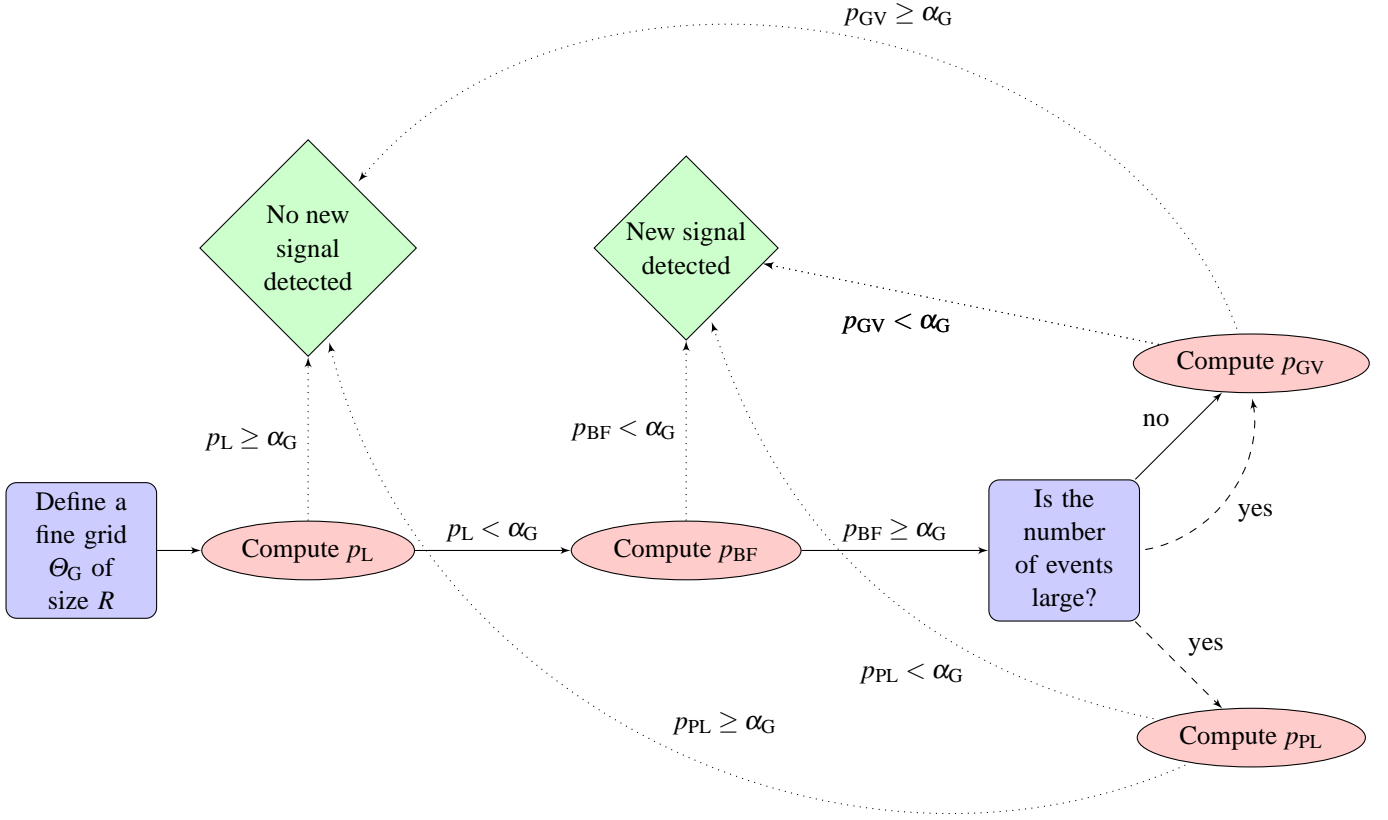


Fig. 4 Outline of the combined approach. General guidelines for one-dimensional statistical signal detections in HEP. Θ_G is the grid of possible locations of the signal over the energy spectrum; its resolution is given by R . p_L is the minimum of the local p-values and p_{BF} its Bonferroni adjusted counterpart. α_G is the predetermined false detection rate. p_{PL} and p_{GV} are the global p-values provided by PL [1, 14] and GV [2] respectively. Dashed arrows indicate that two actions are equally valid, and dotted lines lead to the final conclusion in terms of evidence in favor of the new resonance.

Let $\tilde{\alpha}$ be the false detection rate associated with the combined approach, and consider the events

$$BF_0 = \{\text{Reject } H_0 \text{ at level } \alpha_G \text{ with Bonferroni}\}$$

$$GV_0 = \{\text{Reject } H_0 \text{ at level } \alpha_G \text{ with GV}\}.$$

As in (5) we use $P(\cdot|\eta=0)$ to denote the probability that one event occurs given that the null hypothesis is true, i.e., in absence of the signal. Because the combined approach rejects H_0 when either Bonferroni or GV does so, it follows that

$$\begin{aligned} \tilde{\alpha} &= P(BF_0 \text{ or } GV_0|\eta=0) \\ &= P(BF_0|\eta=0) + P(GV_0|\eta=0) - P(BF_0 \text{ and } GV_0|\eta=0) \\ &= P(BF_0|\eta=0) + P(GV_0|\eta=0) - P(GV_0|BF_0, \eta=0)P(BF_0|\eta=0). \end{aligned}$$

By the ordering of the p-values in (22), if H_0 is rejected by Bonferroni, then it is typically rejected by GV and thus,

$$P(GV_0|BF_0, \eta=0) \approx 1,$$

from which it follows that $\tilde{\alpha} \approx P(GV_0|\eta=0)$, where $P(GV_0|\eta=0)$ is the false detection rate of GV. The power of the combined approach can be obtained in a similar manner by considering the events

$$L_1 = \{\text{Reject } H_0 \text{ at level } \alpha_G \text{ with local p-values}\}$$

$$GV_1 = \{\text{Reject } H_0 \text{ at level } \alpha_G \text{ with GV}\},$$

and evaluating probabilities of the type $P(\cdot|\eta, \theta)$ defined in (5).

To illustrate its statistical properties, we apply the combined approach to a set of 100,000 simulated datasets from the model in Example II with τ fixed at 1.4. For each dataset

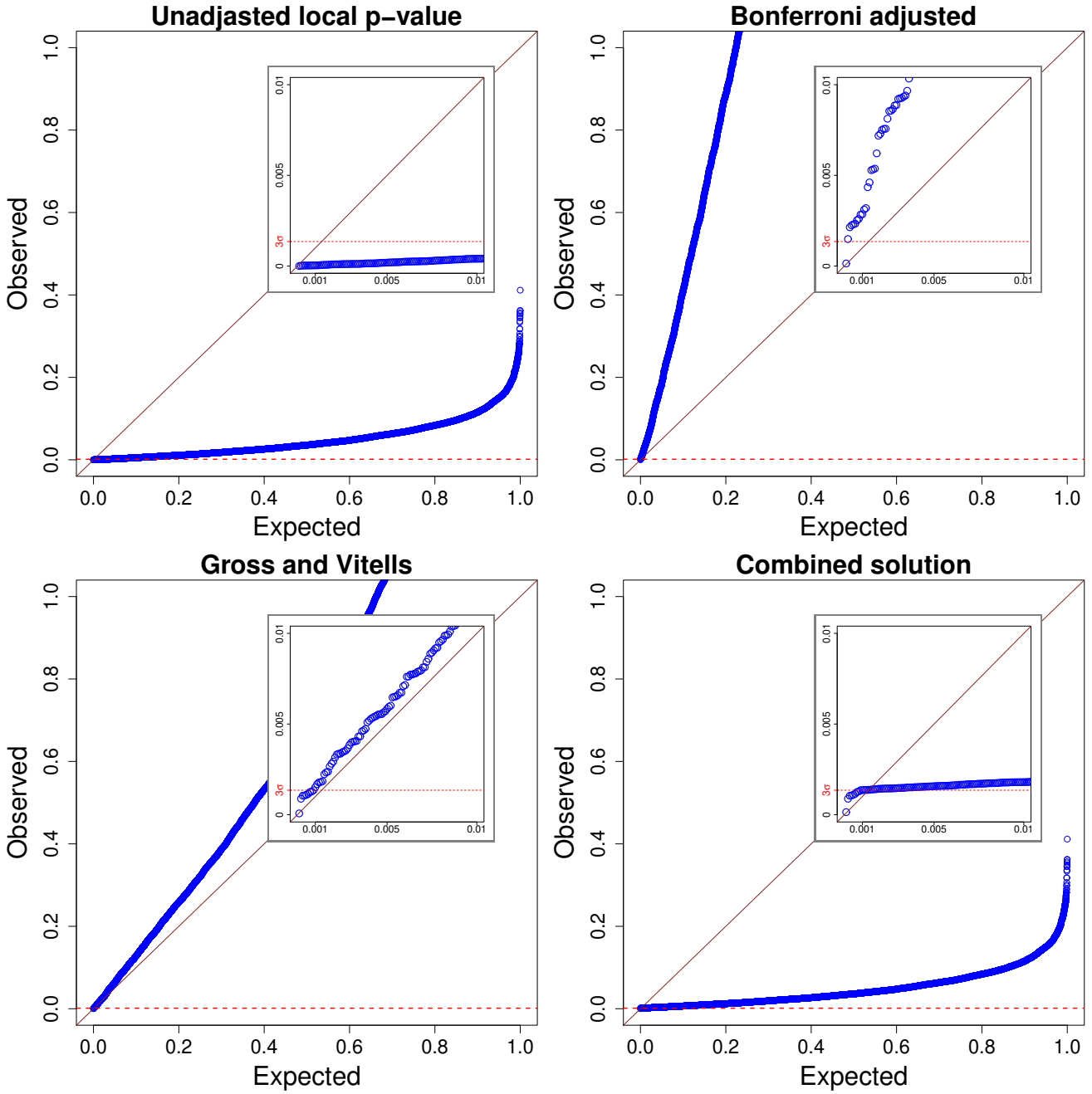


Fig. 5 QQ-plots for the unadjusted local, Bonferroni adjusted and GV p-values computed for the 100,000 simulated background-only datasets from Example II of Section 5. Each dataset considers 2000 background only events. The p-values selected via the combined procedure in Fig. 4 are also reported. Each set of p-values is compared with the expected quantiles of a Uniform distribution on $[0, 1]$. The inlayed plots in each panel magnify the important range of the p-value distributions near zero.

we first simulate 2000 background only events and then we simulate 30 additional events from a Gaussian source centered at 9 GeV. For both the 100,000 background only datasets and the 100,000 background plus source datasets we compute unadjusted local p-values, Bonferroni's corrections, and GV. Table 2 reports the number of times each of the testing procedures considered is selected by the combined approach to make a final decision at the 3σ significance level. The

average computational times for each method are also reported. In the presence of source emission, the most computationally expensive method GV was used only about 44% of the time, leading to a computational gain of about 89 days over the 100,000 simulations. Conversely, in absence of the signal, GV was used about 2.9% of the time, leading to a computational gain of about 155 days. In order to assess the robustness of the method with respect to the desired statisti-

cal properties, we computed the false discovery rate and the power using nominal levels at 3σ significance. The results are presented in Table 3. As discussed above, the combined approach exhibits statistical properties which are approximately equivalent to those of GV (or PL). As expected, the small discrepancies between the two methods are due to the fact that in 0.375% of the replications $p_{GV} > p_{BF}$. When removing these cases from the analysis, both the probability of a Type I error and the power of the combined approach coincide with those of GV.

Finally, Fig. 5 displays the p-values computed with each procedure on each of the 100,000 simulated background-only datasets. Ideally a p-value will follow a uniform distribution on the unit interval under repeated sampling of data under H_0 : this insures that the method will have the target Type I error rate. In the QQ-plots in Fig. 5, the p-values will fall along the 45° line if they follow a uniform distribution. If they deviate above this line, the procedure is conservative and if they deviate below the procedure will exhibit too many false positives. As expected, the unadjusted local p-values are always smaller than their expected values assuming uniform distribution, whereas both Bonferroni and GV are conservative. The combined approach leads to an intermediate situation in which the p-values are over-conservative up to the significance level α_G adopted at each step of the algorithm in Fig. 4 (3σ in Fig. 5), whereas the p-values become under-conservative above α_G , i.e., only for uninteresting cases.

8 Discussion

In this article we investigate the performance of four different testing procedures for the statistical detection of new particles: the multiple hypothesis testing approach, also known as local p-values [6, 7], its Bonferroni adjusted counterpart, the LRT-based approach of Gross and Vitells [2], GV, and the Score-based approach of Pilla et al. [1, 14], PL.

We show analytically that local p-values are strongly affected by the arbitrary choice of the grid resolution, R , over the energy range where the tests are conducted. Specifically, when R is sufficiently large, the unadjusted p-values provide a higher number of false detections than expected, whereas the Bonferroni adjusted local p-values may lead to over conservative inference if R is large. However, as shown in our realistic data analysis, if R is only moderately large ($R = 80$ in our case) Bonferroni represents a reasonable choice. Thus, in order to make final conclusions and to take advantage of the easy implementation of the Bonferroni correction, it should always be used as a preliminary tool in statistical signal detection as described in Section 7.

If the number of search regions R is quite large, a good trade-off is provided by both PL and GV which produce global p-values as a measure of the evidence for a new source

of emission. Although, PL and GV lead to the same conclusions for large sample sizes, based on our simulations, for small samples sizes PL may produce a higher number of false detections than expected, and thus GV is preferable when fewer events are available. From a computational perspective, difficulties may arise with both methods when dealing with complex models; these stem from the required numerical integrations of PL and the Monte Carlo simulations and multidimensional optimization of GV. The latter are not required by PL since the procedure does not require estimation of the signal strength.

PL requires a higher level of mathematical complexity to compute the geometric constants involved. This is exacerbated when free parameters are present under the null model, and the methodology must be extended as in [14]. On the other hand, PL automatically implements the case of multidimensional nuisance parameters under the alternative hypothesis, whereas for GV, the existing multivariate counterpart in [30] does not represent a direct extension of the theory illustrated in this paper. Specifically, the argument based on the number of upcrossings of the LRT process is replaced by the concept of Euler characteristics, which unfortunately does not enjoy the advantages available through the use of the c_0 threshold.

For the classical one-dimensional problem, Section 7 summarizes the methods and provides step-by-step guidelines for a combined approach for statistical signal detection in High Energy Physics. The combined approach preserves both false detection rate and power, while allowing considerable gains in terms of implementation and computational time relative to other methods.

Acknowledgements

JC thanks the support of the Knut and Alice Wallenberg foundation and the Swedish Research Council. DvD acknowledges support from a Wolfson Research Merit Award provided by the British Royal Society and from a Marie-Curie Career Integration Grant provided by the European Commission.

References

1. R. Pilla, C. Loader and C.C. Taylor. *Physical Review Letters*, 95:, Dec 2005.
2. E. Gross and O. Vitells. *The European Physical Journal C*, 70(1-2):525–530, 2010.
3. S.S. Wilks. *The Annals of Mathematical Statistics*, 9: 60–62, 1938.
4. H. Chernoff. *The Annals of Mathematical Statistics*, 25 (3):573–578, 1954.

5. A.C. Davison. *Statistical Models*. Cambridge Series in Statistical and Probabilistic Mathematics. Cambridge University Press, 2003.
6. M. Della Negra, P. Jenni and T.S. Virdee *Science*, 338: 1560–15689, 2012.
7. D.A. van Dyk. *Annual Review of Statistics and Its Application*, 1(1):41–59, 2014.
8. R.O. Kuehl. *Design of Experiments: Statistical Principles of Research Design and Analysis, 2nd Edition*. Cengage, 2000.
9. J. Conrad. *Astroparticle Physics*, 62:165–177, 2015.
10. J.W. Tukey. *Biometrics*, 5(2):99–114, 1949.
11. Y. Benjamini and Y. Hochberg. *Journal of the Royal Statistical Society B*, 57:289–300, 1995.
12. B. Efron. *Large-Scale Inference*. IMS Monographs Cambridge University Press, 2010.
13. S. Mukhopadhyay *Biometrics*, doi: 10.1111/biom.12423.
14. R. Pilla and C. Loader. *arXiv:math/0511503v2 [math.ST]*, 2006.
15. S. Algeri, J. Conrad and D.A. van Dyk. *MNRAS Letters*, 458(1):84–88, 2016.
16. S. Chatrchyan et al. *Physics Letters B*, 716(1):30 – 61, 2012.
17. G. Aad et al. *Physics Letters B*, 716(1):1 – 29, 2012.
18. R.B. Davies. *Biometrika*, 64(2):247–254, 1977.
19. R.B. Davies. *Biometrika*, 74(1):33–43, 1987.
20. R.J. Adler. *The Annals of Applied Probability*, 10(1): 1–74, 2000.
21. V.L. Kashyap, D.A. van Dyk, A. Connors, P.E. Freeman, A. Siemiginowska, J. Xu and A. Zezas *The Astrophysical Journal*, 719 :900–914, 2010.
22. B. Efron and R.J. Tibshirani. *An Introduction to the Bootstrap*. Chapman & Hall/CRC, 1993.
23. W. B. Atwood et al. *The Astrophysical Journal*, 697(2): 1071, 2009.
24. M. Ackermann et al. *Physical Review D*, 91122002, 2015.
25. C. Weniger *Journal of Cosmology and Astroparticle Physics* , 08: 007, 2012.
26. B. Anderson, S. Zimmer, J. Conrad, M. Gustafsson, M. Sanchez-Conde and R. Caputo *Journal of Cosmology and Astroparticle Physics* , 02: 026, 2016.
27. M.A. Sanchez-Conde and F. Prada *Monthly Notices of the Royal Astronomical Society*, 442(3):2271–2277, 2014.
28. S. Algeri, D.A. van Dyk and J. Conrad. "Testing one hypothesis multiple times". *In preparation*, 2016.
29. G.J. Feldman and R.D. Cousins. *Physical Review D*, 57: (7):penalty0 3873 – 3889, 1998.
30. O. Vitells and E. Gross. *Astroparticle Physics*, 35(5): 230 – 234, 2011.

